Available online at www.sciencedirect.com
ScienceDirect
Journal of Solid State Chemistry 180 (2007) 2785–2789
JOURNAL OF SOLID STATE CHEMISTRY
www.elsevier.com/locate/jssc

Formation of tetragonal hydrogen tungsten bronze by reactive mechanical alloying

G. Urretavizcaya[a,*], F. Tonus[b], E. Gaudin[b], J.-L. Bobet[b], F.J. Castro[a]

[a]Centro Atómico Bariloche (CNEA, CONICET), Instituto Balseiro (UNC), Av. Bustillo 9500, R8402AGP, S.C. de Bariloche, Argentina
[b]Institut de Chimie de la Matière Condenseé de Bordeaux (ICMCB), CNRS (UPR 9048), Université de Bordeaux I, 87 Avenue du Dr. A. Schweitzer, 33608 Pessac Cedex, France

Received 13 June 2007; received in revised form 9 August 2007; accepted 10 August 2007
Available online 25 August 2007

Abstract

Hydrogen tungsten bronzes have been synthesized by reactive mechanical alloying monoclinic tungsten (VI) oxide under hydrogen atmosphere. Two milling devices with different energy ranges were used. Regardless of the distinct reaction times, a similar phase evolution was observed with both apparatus. The characterization of the materials was performed by XRD, SEM, DSC and total hydrogen content determination. The final product obtained was a mixture of tetragonal $H_{0.33}WO_3$ and $H_{0.23}WO_3$ bronzes.
© 2007 Elsevier Inc. All rights reserved.

Keywords: Hydrogen tungsten bronze; Mechanical alloying; Hydrogen absorption

1. Introduction

Tungsten bronzes are non-stoichiometric materials in which an electropositive element is incorporated into the structure of tungsten (VI) oxide to form compounds of chemical formula M_xWO_3, with x in the range 0–1. Several electropositive elements can form tungsten bronzes by intercalation among the WO_6 octahedra. Alkaline metal bronzes are the most studied bronzes [1,2], but also alkaline earth metals, transition metals [1], rare earths [1,3] and hydrogen [4–13] have been incorporated into the WO_3 structure. These materials show a very rich crystallographic chemistry and very interesting electronic properties due to its metallic conductivity, produced by the electron mobility. Most of the applications are concentrated on the electrochromic properties. As a characteristic property, tungsten bronzes show intense colors (e.g. the full range of the visible spectra can be covered) depending on the proportion and type of electropositive element present in the compound.

Hydrogen tungsten bronzes are materials in which the hydrogen content can vary from 0.1 to 0.6. They exhibit several crystallographic structures at room temperature: orthorhombic bronzes with $x = 0.1$ [4,10], tetragonal bronzes with $x = 0.23$ and 0.33 [4,5,7], hexagonal bronzes with $x = 0.24$ [8,11] and cubic bronzes with $x = 0.53$ [6,9]. In particular, regarding the tetragonal structures, two different phases were reported: tetragonal B ($0.15 < x < 0.23$) and tetragonal A ($0.33 < x < 0.5$) [5,7]. The first method used to obtain hydrogen bronzes was the reaction of tungsten (VI) oxide with nascent hydrogen produced by reaction of zinc with hydrochloric acid [4,5]. The structure of the hydrogen tungsten bronze obtained by this synthesis pathway is tetragonal. Later, hexagonal hydrogen tungsten bronze was prepared by reaction of Cu + monoclinic WO_3 to form $CuWO_4$, reduction under hydrogen flow to lead to H_xWO_3 + Cu, and free metal elimination and washing with concentrated nitric acid [11]. More recently, the mechanochemical synthesis route has been successfully used for bronze formation, by milling m-WO_3 with liquid hydrocarbons (e.g. xylene) under air [13]. In this case the hydrocarbons are the source of hydrogen, and the tetragonal structure is obtained. The mechanochemical route was also used to obtain sodium tungsten bronze by milling Na + m-WO_3 under Ar [2].

In this paper we report the direct formation of tetragonal hydrogen bronzes by reactive mechanical alloying (RMA) of monoclinic WO_3 in a powder form under hydrogen

*Corresponding author. Fax: +54 2944 445199.
E-mail address: urreta@cab.cnea.gov.ar (G. Urretavizcaya).

0022-4596/$ - see front matter © 2007 Elsevier Inc. All rights reserved.
doi:10.1016/j.jssc.2007.08.007

atmosphere. This synthesis method has been widely applied to enhance the kinetics of solid–gas reactions. For example, metallic hydrides have been obtained by milling under hydrogen atmosphere [14–17], nitrides have been formed by milling under nitrogen [18,19], and mixtures of oxides and nitrides have been obtained by RMA under air [19]. Basically, with RMA, the interaction of a solid material with a gaseous phase is improved by several processes induced by ball milling: particle size reduction, introduction of defects, repeated cold welding and formation of highly reactive fresh surface.

Additionally, we compare here two milling devices with different energy ranges. The main advantage of a high-energy mill is its efficiency. Typically, shorter processing times are required with high-energy milling. On the other hand, the main advantage of a low-energy mill is the possibility of observing intermediate stages of the mechanochemical treatment. These intermediate stages usually cannot be observed with a high-energy device.

2. Experimental

Monoclinic WO_3 (Aldrich 99%) was milled under 500 kPa H_2 at room temperature. Two different mills were used: a low-energy mill (Uni-Ball Mill II, Australian Scientific Instruments) and a high-energy mill (Pulverissette 5, Fritsch). In the first one, the ball to powder mass ratio, the rotation speed and the total milling time were 20/1, 196 rpm and 200 h, respectively. In the planetary mill they were 20/1, 250 rpm and 10 h, respectively. At regular intervals a small amount of powder was removed from the container within a glove box to follow the evolution of the milled powder by X-ray diffraction (XRD), differential scanning calorimetry (DSC), scanning electronic microscopy (SEM) and hydrogen uptake determination. The X-ray powder diffraction analysis was performed using a Philips PW 1710/01 instrument with Cu$K\alpha$ radiation and graphite monochromator. XRD runs were performed under argon atmosphere, using a hermetic sample-holder with Mylar window. The thermal behavior of the samples was studied by DSC (DSC 2910, TA Instruments) at a heating rate of 10 K/min under Ar flow (122 cm^3/min). Microstructural characterization was done using a SEM 515, Philips Electronic Instruments equipment. Elemental identification was made by energy dispersive X-ray analysis (EDS, Philips Electronic Instruments). The total hydrogen content was determined after fusion and decomposition of the samples using a LECO RH-404 instrument.

3. Results and discussion

As will be discussed later, similar results (with different processing times) were obtained using the low- and high-energy mills. In the following, we present the results of the low-energy milling process.

A first indication of phase evolution during milling was obtained by simple visual examination of the powder. With the mechanochemical treatment, the color of the material changed from the pale greenish yellow of the starting oxide to a deep blue characteristic of the hydrogen tungsten bronzes.

A more detailed analysis of the evolution was done by XRD (Fig. 1). The starting material was indexed as pure monoclinic WO_3 (JCPDS powder diffraction card no. 42-1035). After 15 h of milling, the diffraction pattern changes, showing broadened reflections consequence of the mechanochemical treatment and due to crystallite size reduction, introduction of defects and deformation of the powder. Also at this milling time, the presence of tetragonal $H_{0.23}WO_3$ bronze (JCPDS powder diffraction card no. 42-1261) can be detected for the first time. From 15 to 50 h of milling time, the reflections of $H_{0.23}WO_3$ grow whereas those of monoclinic WO_3 decrease in intensity, just to almost disappear at 50 h. After 100 h of mechanochemical treatment, the first indications of the formation of $H_{0.33}WO_3$ bronze (JCPDS powder diffraction card no. 23-1449), start to appear: a small change in the position of the most intense reflection centered in $2\Theta = 24^\circ$, the reduction of the reflection of $H_{0.23}WO_3$ located around $2\Theta = 23^\circ$, and the change of shape of the

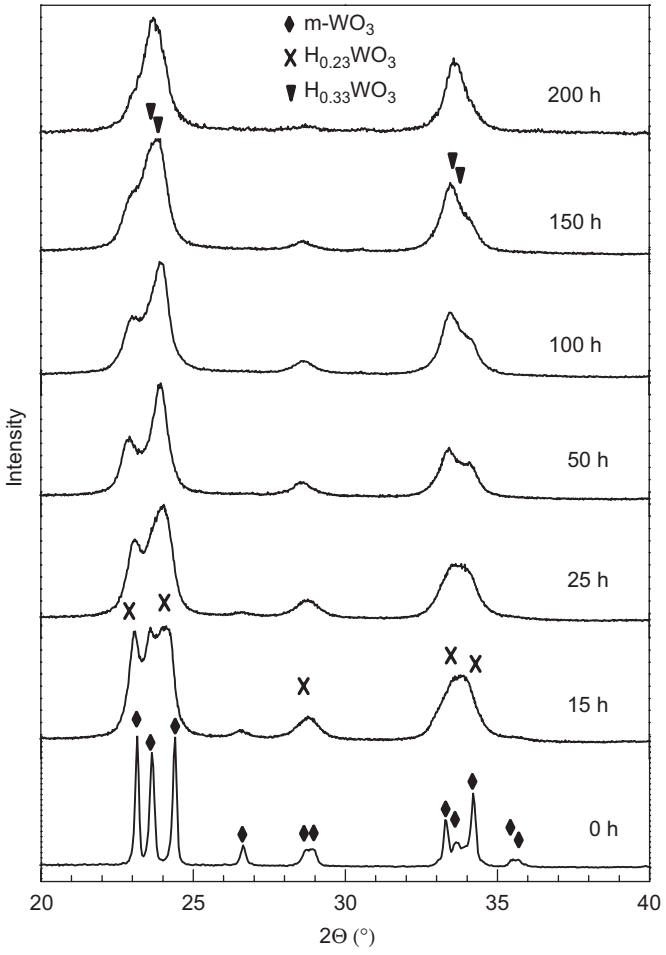

Fig. 1. Selected regions of the XRD patterns of WO_3 milled different times with the low-energy mill. The pattern corresponding to the starting material (0 h) is also shown.

peaks of the $2\Theta = 33$–34° range. From 100 to 200 h of milling, this transformation is accentuated. After 200 h of milling, a mixture of both hydrogen tungsten bronzes, with a greater proportion of $H_{0.33}WO_3$ is obtained. The presence of a small amount of cubic hydrogen tungsten bronze (JCPDS powder diffraction card no. 42-1260) cannot be discarded because its reflections coincide with some reflections of the tetragonal bronze.

A small contamination with Fe from the milling tools was detected by EDS (<1%, wt%) and observed by XRD as a small peak that can be assigned to the more intense reflection of $FeWO_4$ ($2\Theta = 30.5^\circ$, JCPDS card number 85-1354) in the samples milled 100 h or longer.

As mentioned before, a similar evolution was observed when milling was performed using the high-energy planetary mill. In this case, due to the more energetic conditions of the process, the milling time required to obtain the tetragonal hydrogen tungsten bronze was shorter. After 1 h of milling time $H_{0.23}WO_3$ bronze is already detected in the sample, and 10 h of mechanical treatment are enough to obtain a product similar to that obtained after 200 h of low-energy milling. Then, considering the formation rate of H_xWO_3, it is possible to establish an approximate relationship between the efficiency of both milling apparatus: 1 h of milling in the planetary mill is equivalent to nearly 20 h of milling in the low-energy device.

Comparing with previously reported results [13], the mechanical treatment under hydrogen atmosphere seems to be more effective than milling the material with hydrocarbons under air. In this last case it took 12 h to obtain $H_{0.23}WO_3$, whereas we obtained a product with a higher amount of hydrogen (a mixture of $H_{0.23}WO_3$ and $H_{0.33}WO_3$) after 10 h of high-energy milling. Moreover, by milling under hydrogen atmosphere, the product is not mixed with residual organic solvents.

The morphological evolution of the material is illustrated by the SEM images of Fig. 2. The starting material shows a wide particle size distribution, with particles in the 10–100 μm range (Fig. 2A). After 5 h of milling (Fig. 2B and C), a noticeable decrease in size occurs. Particles with sizes lower than 1 μm can be seen mixed with bigger particles (10–20 μm). By further milling, the reduction of particle size continues. Very fine submicrometric particles (<0.1 μm) can be observed forming agglomerates of several microns (Fig. 2D and E), probably a consequence of the phenomenon of cold welding, characteristic of the ball milling process. The same observation about the morphology of the powders can be done on the powders ball milled with the planetary mill. It confirms the previous equivalence (i.e. 1 h of planetary mill = 20 h of low-energy device) reported from XRD analysis. However, it should be noticed that the powder obtained with the planetary mill usually exhibits a less smooth shape.

DSC measurements under argon flow were performed in order to characterize the thermal behavior of the samples. In Fig. 3, the curves corresponding to the samples milled 50 and 200 h are shown. An extended endothermic peak starting at approximately 35 °C and finishing at 390 °C is observed. In agreement with Dickens et al. [7], this endothermic event is attributed to hydrogen bronze decomposition, according to the reaction:

$$H_xWO_{3(s)} = \frac{x}{2}H_{2(g)} + WO_{3(s)}$$

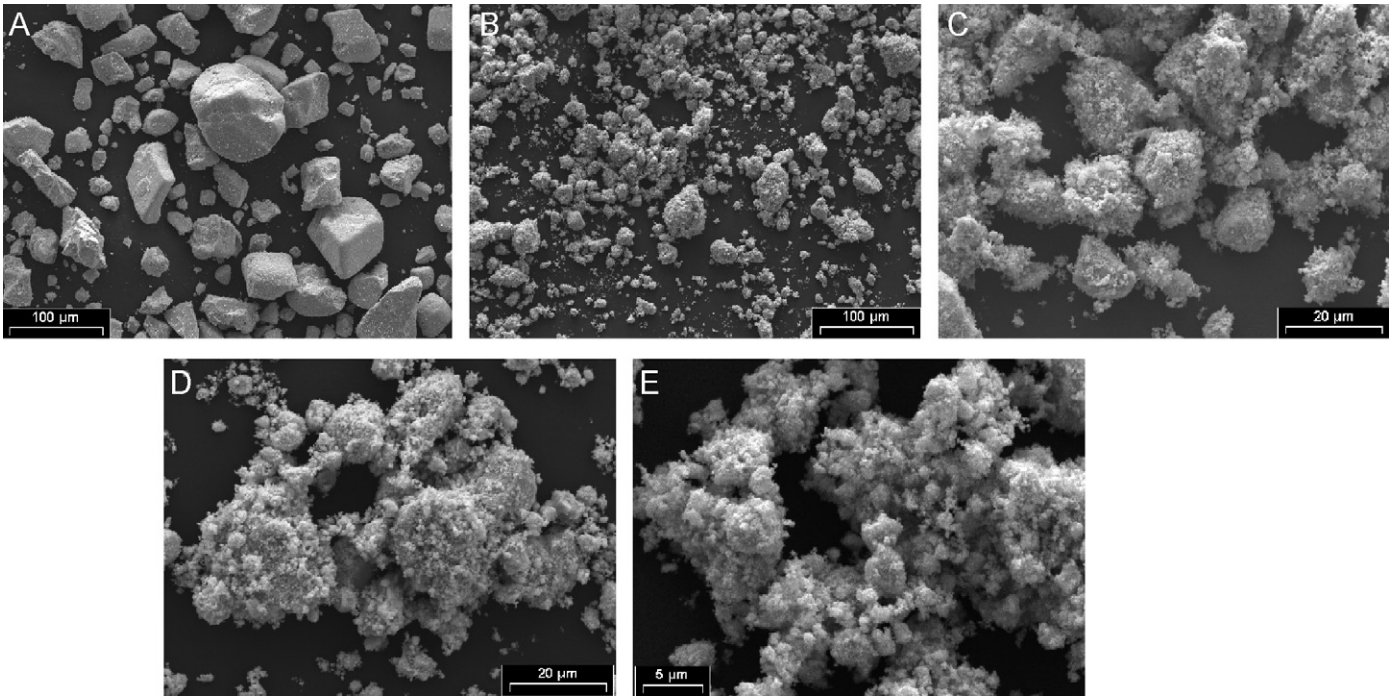

Fig. 2. SEM micrographs of m-WO_3 without milling (A) and after RMA with the low-energy mill: 5 h (B and C), 15 h (D) and 200 h (E).

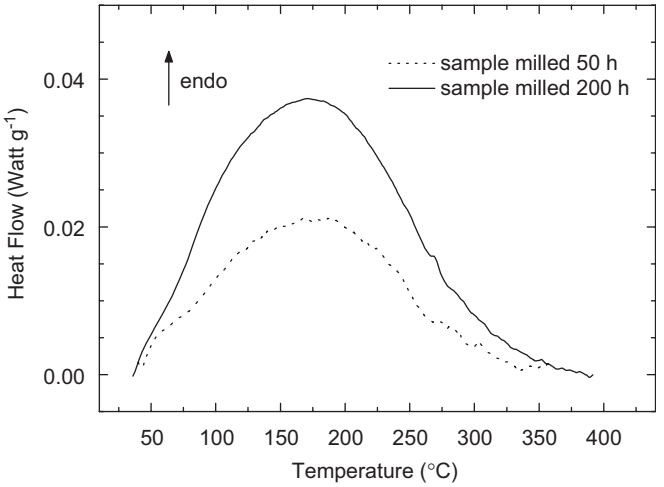

Fig. 3. DSC curves of WO_3 milled 50 h (dotted line) and 200 h (solid line) under H_2 with the low-energy mill.

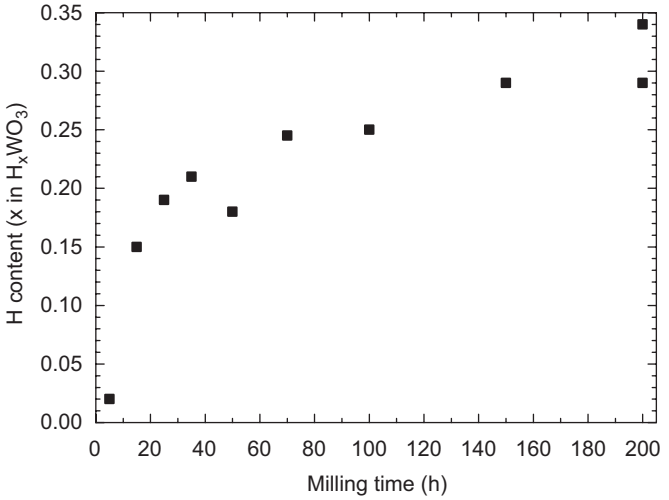

Fig. 4. Hydrogen content determined from the DSC measurement as a function of milling time (low-energy mill).

The maximum of the DSC peak is located at 170 °C. This is in rather good agreement with the value estimated by Dickens et al. [7] who performed calculations of the thermodynamic stability of the tetragonal hydrogen bronze and predicted an approximated decomposition temperature for $H_{0.35}WO_3$ equal to 176 °C. The temperature range in which the bronze obtained by ball milling decomposes under argon flow is approximately twice wider and starts nearly 170 °C below the temperature of the vacuum decomposition observed for the bronze synthesized by reduction of WO_3 with nascent H_2 (200–400 °C) [7]. In addition to the different conditions of the measurements, the change in the decomposition temperature range could be attributed to the effect of mechanical milling and the presence of a mixture of phases. It is widely known that RMA produces a particular microstructure with small particle and crystallite sizes and a high concentration of defects [19]. As an example, in the case of hydride-forming materials, such as Mg, this microstructure produces a substantial lowering of the hydride decomposition temperature [15,17]. On the other hand, the particular microstructure together with the presence of a mixture of bronzes can explain the width of the DSC curves.

The enthalpy associated with the endothermic process has been estimated from the area of the DSC peak. In our study, this area grows with milling time, reflecting an increase of hydrogen content in the material. In order to quantify the amount of hydrogen in the bronzes, we related the measured areas with the enthalpies of formation of tetragonal $H_{0.35}WO_3$ and $H_{0.18}WO_3$ bronzes determined by Dickens et al. [7]. These enthalpies are -9.6 ± 0.8 and -4.8 ± 0.6 kJ/mol, respectively, and give values of enthalpies per mole of atomic hydrogen equal to -27.4 ± 2.3 and -26.7 ± 3.3 kJ/mol H, respectively. The similarity of these values suggests that there are no significant differences between the binding energies of hydrogen in these phases. This similarity allows us to use a mean value of formation enthalpy per mol of atomic hydrogen for a generic H_xWO_3 equal to $-27x$ kJ/mol, irrespective of x, and to determine the value of x as a function of milling time from the area under the DSC curves.

From the obtained values of x (Fig. 4), two milling stages can be identified. During the first 40 h of milling (with the low-energy device), the rate of incorporation of hydrogen into the material is high. This stage finishes with an x value around 0.20, and coincides with the formation of $H_{0.23}WO_3$ observed by XRD analysis and with the noticeable particle size reduction shown before. The particle size reduction and the incorporation of strains and defects due to mechanical milling enhance the interaction of hydrogen with the material and favor its incorporation. These effects have been previously observed in several systems [14–19]. In the second stage (i.e. from 40 to 200 h), hydrogen is incorporated with a rate 10 times lower, and the x value goes from 0.20 to around 0.30–0.35. This stage corresponds to the formation of $H_{0.33}WO_3$ from $H_{0.23}WO_3$. In agreement with the presence of a mixture of tetragonal bronzes with hydrogen content equal to 0.23 and 0.33 atoms per mole observed by XRD, the amount of hydrogen calculated in this case is a value between these two limits. The values of x determined by DSC were corroborated by measuring the total amount of hydrogen in the samples by using the LECO equipment. As an example, for the 200 h-milled sample we obtained an x value equal to 0.28 with the LECO equipment.

The tetragonal bronze obtained by ball milling is very sensitive to air. When hydrogen determination by LECO was performed on samples previously exposed to air, the hydrogen content measured was lower than the one calculated from DSC or determined by LECO on a sample with a short time of exposure to air (just the time needed to introduce the sample into the equipment). The partial degradation of the material under air was also observed by

a change in color from brilliant deep blue into a blackish blue, and also by changes in the XRD patterns indicating bronze decomposition.

4. Conclusions

RMA under hydrogen atmosphere has been used to synthesize tetragonal hydrogen tungsten bronzes from monoclinic tungsten (VI) oxide. The bronze formed during the first stages of the milling was $H_{0.23}WO_3$. With further milling the incorporation of hydrogen continued and $H_{0.33}WO_3$ was synthesized. The final product was a mixture of both tetragonal bronzes. A similar evolution of the material was observed using two different ball milling apparatus with high and low-energy ranges, but distinct milling times were required in each case.

Acknowledgments

The authors thank H.L. Corso for technical assistance with LECO measurements. They also thank the Cooperation Program ECOS-SECyT (France-Argentine) for partial financial support to carry out this work.

References

[1] P. Hagenmuller, Comprehensive Inorganic Chemistry. Tungsten bronzes, Vanadium bronzes, and Related Compounds, vol. 4, Pergamon Press, Oxford, 1973, pp. 541–605 (Chapter 50).
[2] J. Wang, G. Liu, Y. Du, Mater. Lett. 57 (2003) 3648–3652.
[3] W. Ostertag, Ch.V. Collins, Mater. Res. Bull. 2 (1967) 217–221.
[4] O. Glemser, C. Naumann, Z. Anorg. Allg. Chem. 265 (1951) 289.
[5] P.G. Dickens, R.J. Hurdicht, Nature 215 (1967) 1266–1267.
[6] P.J. Wiseman, P.G. Dickens, J. Solid State Chem. 6 (1973) 374–377.
[7] P.G. Dickens, J.H. Moore, D.J. Neild, J. Solid State Chem. 7 (1973) 241–244.
[8] M.V. Susic, Y.M. Solonin, J. Mater. Sci. 23 (1988) 267–271.
[9] L.A. Aleshina, L.Y. Berezin, N.B. Inyushin, V.P. Malinenko, A.D. Fofanov, Sov. Phys. Solid State 31 (1989) 2048–2053.
[10] E. Cazzanelli, C. Vinegoni, G. Mariotto, A. Kuzmin, J. Purans, Solid State Ionics 123 (1999) 67–74.
[11] Y.M. Solonin, O.Y. Khyzhun, E.A. Graivoronskaya, Cryst. Growth Design 1 (2001) 473–477.
[12] M.S. Whittingham, Solid State Ionics 168 (2004) 255–263.
[13] S. Takai, N. Hoshimi, T. Esaka, Electrochemistry 72 (2004) 876–879.
[14] Y. Chen, J.S. Williams, J. Alloys Compds. 217 (1995) 181–184.
[15] A. Zaluska, L. Zaluski, J.O. Ström-Olsen, J. Alloys Compds. 289 (1997) 197–206.
[16] J.L. Bobet, C. Even, Y. Nakamura, E. Akiba, B. Darriet, J. Alloys Compds. 298 (2000) 279–284.
[17] F.C. Gennari, F.J. Castro, G. Urretavizcaya, J. Alloys Compds. 321 (2001) 46–53.
[18] A. Calka, J.S. Williams, Mater. Sci. Forum 88–90 (1992) 787–794.
[19] C. Suryanarayana, Prog. Mater. Sci. 46 (2001) 1–184.